Earth System Dynamics

Open Access

Discussions

Continued increase in atmospheric CO_2 seasonal amplitude in the 21st century projected by the CMIP5 Earth System Models

F. Zhao[1] and N. Zeng[1,2]

[1]Department of Atmospheric and Oceanic Science, University of Maryland, USA
[2]Earth System Science Interdisciplinary Center, University of Maryland, USA

Correspondence to: N. Zeng (zeng@atmos.umd.edu)

Discussion Paper | Discussion Paper | Discussion Paper | Discussion Paper |

ESDD

5, 779–807, 2014

CMIP5 Earth System Models

F. Zhao and N. Zeng

Title Page

Abstract | Introduction
Conclusions | References
Tables | Figures

◄◄ | ►►
◄ | ►
Back | Close

Full Screen / Esc

Printer-friendly Version

Interactive Discussion

Abstract

Superimposed on the continued increase in the atmospheric CO_2 concentration is a prominent seasonal cycle. Ground-based and aircraft-based observation records show that the amplitude of this seasonal cycle has increased. Will this trend continue into future? In this paper, we analyzed simulations for historical (1850–2005) and future (RCP8.5, 2006–2100) periods produced by 10 Earth System Models participating the Fifth Phase of the Coupled Model Intercomparison Project (CMIP5). Our results show a model consensus that the increase of CO_2 seasonal amplitude continues throughout the 21st century. The seasonal amplitude of the multi-model global mean detrended CO_2 increases from 1.6 ppm during 1961–1970 to 2.7 ppm during 2081–2090, and the mean relative amplitude increases by 62 ± 19 %. This increase is dominated by a 68 ± 25 % increase from Net Biosphere Production (NBP). We then show the increase of NBP amplitude mainly comes from enhanced ecosystem uptake during Northern Hemisphere growing season under future CO_2 and temperature conditions. Separate analyses on net primary production and respiration reveal that enhanced ecosystem carbon uptake contributes to about 75 % of the amplitude increase. Stimulated by higher CO_2 concentration and high-latitude warming, enhanced net primary production likely outcompetes increased respiration at higher temperature. Zonal distribution and the spatial pattern of NBP change suggest that regions north of $45°$ N dominate the amplitude increase. We also found that changes of NBP and its seasonal amplitude are significantly ($R = 0.73$, $p < 0.05$) correlated – models that simulate a stronger carbon uptake tend to show a larger change of NBP seasonal amplitude.

1 Introduction

Since 1958, nearly continuous measurement of atmospheric CO_2 concentration has been taken at Mauna Loa, Hawaii ($19.5°$ N, $155.6°$ W, 3400 m altitude), which is located within the well-mixed trade wind belt. Its record captures the CO_2 increase from below

320 ppm to over 400 ppm today. Superimposed upon this upward trend is a prominent seasonal cycle that has been primarily attributed to the seasonal imbalance of growth and decay of the Northern Hemisphere biosphere. At Mauna Loa (MLO), CO_2 reaches maximum in May and minimum in October with a peak-to-trough amplitude of about 6 ppm, which has been shown to represent a close average of a large portion of the Northern Hemisphere biosphere (Kaminski et al., 1996), where the amplitude ranges from 3 ppm at 10° N to 15 ppm at Point Barrow, Alaska (71° N). Early studies has speculated that global primary production would decrease because of global changes such as acid rain and cutting forest (Whittaker and Likens, 1973; Reiners, 1973), in which case we might observe a reduction of CO_2 seasonal amplitude (assuming changes in respiration are similar at the peak and trough of the CO_2 seasonal cycle). However, Hall et al. (1975) found no evidence of a long-term change in amplitude from 15 years of MLO CO_2 record (1958–1972). They concluded either the biosphere is too big to be affected yet or the degradation of biosphere is balanced by enhanced CO_2 fertilization and increased use of fertilizers in agriculture.

As the industrialization processes expanded during the 1970s and 1980s, it seems likely that the metabolic activity of the biosphere became stronger, as indicated by a rapid increase in CO_2 seasonal amplitude computed from MLO CO_2 record (Pearman and Hyson, 1981; Cleveland et al., 1983; Bacastow et al., 1985). Enhanced CO_2 fertilization was considered as an obvious factor, and a change to climatic conditions a possible cause (Bacastow et al., 1985). Keeling et al. (1996) further linked the amplitude increase with climate change by showing the two-year phase lag relationship between trends in the relative amplitude and trends in 30–80° N mean temperature. They suggest the warming may also lead to a lengthening of growing season associated with phase advances of about 7 days during the declining phase of the seasonal cycle.

Unlike CO_2 fertilization, the combined effect of climate (temperature, precipitation, etc.) introduces strong interannual variability to the amplitude change, and changes in climate could either lead to an amplitude increase or decrease – it was noticed later

CMIP5 Earth System Models

F. Zhao and N. Zeng

that despite of the continuing rise of 30–80° N mean land temperature since 1990s, CO_2 seasonal amplitude at MLO has declined. Buermann et al. (2007) attributed the decline to the severe drought in North America during 1998–2003. They reasoned that MLO receives mainly Eurasian air masses in the Northern Hemisphere winter but relatively more North American air masses in summer. A decreasing trend in the 1990s was observed at Point Barrow, Alaska.

After the mid-1990s, the increasing trend of amplitude resumed at MLO. The latest analysis by Graven et al. (2013) shows a 16 % increase in MLO amplitude and a 30 % increase in Point Barrow amplitude over the 1958–2011 period. They compared aircraft measurements taken at 500 mb and 700 mb heights in 1958–1961 and 2009–2011, and these data suggest an even larger ($\sim$ 50 %) increase of atmospheric CO_2 seasonal amplitude north of 45° N. They also applied two atmospheric transport models to estimate CO_2 amplitude using monthly Net Ecosystem Production (NEP) from the historical simulation (Exp3.2) results of eight Coupled Model Intercomparison Project Phase 5 (CMIP5) models. Compared with aircraft data, they found the CMIP5 models simulated a much lower amplitude increase.

So far, the magnitude of global amplitude change is not clear. Even though the Global Monitoring Division of NOAA/Earth System Research Laboratory (ESRL) has measured carbon dioxide for several decades at well over 100 surface CO_2 monitoring sites (Conway et al., 1994), fewer than 20 of them have over 30 years of record. ESRL provides a global monthly mean CO_2 time series since 1980, computed from 43 remote stations that sample well-mixed marine boundary layer (MBL). Another source of estimate is from atmospheric inversions, which give spatially explicit surface fluxes in addition to global mean. However, their resolution and accuracy are inherently limited due to a small number of stations used, and errors in atmospheric transport.

Process-based Terrestrial Biosphere Models (TBMs) can generate surface fluxes over the past century or longer, usually with a spatial resolution of half to three degrees. They offer insights in better understanding the mechanisms for the amplitude change. McGuire et al. (2001) compared the relative change of the seasonal amplitude of total

land-atmosphere carbon flux north of 30° N for four TBMs, and they found the trend was overestimated by one of the four models and underestimated by the other three. They suggest the observed trend may be a consequence of the combined effects of rising CO_2, climate variability and land use changes, which has also been noted in previous studies (Kohlmaier et al., 1989; Keeling et al., 1995, 1996; Randerson et al., 1997, 1999; Zimov, 1999). Models show varied extent of amplitude increase, which is likely due to their different sensitivities to CO_2 concentration and climate. It is especially interesting that while Graven et al. (2013) found CMIP5 models might underestimate the amplitude, previous observation indicated the models might overestimate CO_2 fertilization effect (Piao et al., 2013), suggesting that our understanding of the CO_2 seasonal amplitude problem is still limited.

With temperature rise and CO_2 increase, we may see further lengthening of growing season over high latitudes. On the other hand, the atmospheric circulation patterns will also change; the frequency and/or duration of heat waves are very likely to increase over most land areas, and the Increases in intensity and/or duration of drought and flood are likely (International Panel on Climate Change, 2013). It is not clear whether the net effect of natural and human-induced environmental changes would result in an increase or decrease of the amplitude in the future. In this study, we analyzed the fully coupled CMIP5 earth system model runs as part of the Fifth Assessment Report (AR5) of the United Nations' Intergovernmental Panel on Climate Change (IPCC). Specifically, we looked into the emission-driven simulations, which include many of the aforementioned processes and feedbacks. Our goal is to answer the following questions: how does CMIP5 models predict the amplitude and phase changes of CO_2 seasonal cycle in the future? Is it driven mostly by changes in production or respiration? Where the models predict the largest amplitude changes will occur?

Section 2 describes the CMIP5 experiments, models used and our analyzing method; Sect. 3 presents the major results of our multi-model analyses; Sect. 4 discusses and concludes our main findings.

2 Method

2.1 Model descriptions

We analyzed historical and future emission-driven simulation results from 10 CMIP5 ESMs. The historical simulations, referred to as experiment 5.2 or ESM historical 1850–2005 run (Taylor et al., 2012), were forced with gridded CO_2 emissions reconstructed from fossil fuel consumption estimates (Andres et al., 2011). Unlike the concentration-driven (no feedback on CO_2 concentration in the atmosphere) future simulations with four different Representative Concentration Pathways (RCPs), the emission-driven future simulations, referred to as experiment 5.3 or ESM RCP8.5 experiment 2006–2100, were forced with projected CO_2 emissions, following only one scenario – RCP8.5 (Moss et al., 2010). We chose the emission-driven runs because the fully coupled ESMs in these runs have interactive carbon cycle component that can simulate climate-carbon cycle feedback mechanisms. Global atmospheric CO_2 concentrations are simulated prognostically, therefore they reflect the total effect of all the physical, chemical, and biological processes on Earth, and their interactions and feedbacks with the climate system. We obtained model output primarily from the Earth System Grid Federation (ESGF), an international network of distributed climate data servers (Williams et al., 2011). For the GFDL model, we directly retrieved the output from GFDL's Data Portal (http://nomads.gfdl.noaa.gov:8080/DataPortal/cmip5.jsp). The main characteristics of the 10 models are listed in Table 1.

2.2 Analysis procedure

We first analyzed the monthly output of prognostic atmospheric CO_2 concentrations to evaluate the change of CO_2 seasonal amplitude (defined as max minus min of de-trended seasonal cycle) from 1961 to 2099. Atmospheric CO_2 was obtained primarily as the area- and pressure-weighted mean of CO_2 across all vertical levels – a better representation of atmospheric carbon content than surface CO_2. The INM-CM4 model

does not provide CO_2 concentration, so we converted its total atmospheric mass of CO_2 to mole fraction. We excluded the IPSL model from analyses in Sects. 3.1 and 3.2 because its CO_2 output is not available. Only CanESM2 provides three different realizations for both historical and future runs, and we simply use its first realization in our comparison. We believe this choice would lead to a more representative result than including all realizations of CanESM2 in multi-model averaging.

To extract the CO_2 seasonal cycle from the monthly records, we applied the curve-fitting procedures using the CCGCRV software developed at the National Oceanic and Atmospheric Administration Climate Monitoring and Diagnostics Laboratory (Thoning et al., 1989; http://www.esrl.noaa.gov/gmd/ccgg/mbl/crvfit/crvfit.html). This algorithm first fits the long-term variations and the seasonal component in the monthly CO_2 record with a combination of a trend function and a series of annual harmonics. Then the residuals are filtered with fast Fourier transform and transformed back to the real domain. Specifically, we followed the default setup of a quadratic polynomial for the trend function, a four-yearly harmonics for the seasonal component, and long/short-term cutoff values of 650 days/80 days for the filtering in our analyses. We examined the phase change of CO_2 detrended seasonal cycle by counting how frequent the maximums and minimums occur in different months. We used two definitions of seasonal amplitude in our analyses that yield similar results: one directly comes from the CCGCRV package, and another definition is simply max minus min of detrended seasonal cycle in each year. For each model's monthly global mean CO_2, we first computed the detrended CO_2 seasonal cycle as the annual harmonic part plus the filtered residue using the short-term cutoff value. Then we started to investigate the global carbon budget in each model:

$$\frac{dCO_2}{dt} = FFE - NBP + FOA. \tag{1}$$

The left term is the change of CO_2 concentration (or CO_2 growth rate), which we simply computed as the difference between the current month and previous month's concentration – this leads to a half-month shift earlier than the results indicate. The

right side comprises of fossil fuel emission (FFE), net biosphere production (NBP, or net terrestrial-atmosphere carbon exchange, positive if land is a carbon sink) and net ocean-atmosphere flux (FOA, positive if ocean releases carbon). Previous studies have limited the impact of FFE and FOA on trends in CO_2 amplitude to less than a few per-cent change (Graven et al., 2013). Therefore we focused on examining the seasonal cycle of NBP in this study.

For each model, we checked and ensured that the sum of individual flux terms in Eq. (1) equals to the CO_2 growth rate. However, further breakdown of NBP may look very different. For example, the GFDL-ESM2m model's NBP has component fluxes including Net Primary Production (NPP), heterotrophic respiration (R_h), fluxes from land use change (fLuc), fire (fFire), harvest (fHarvest) and grazing (fGrazing). In contrast, NBP approximately equals to NPP minus R_h in CanESM2. To investigate whether the amplitude change is mostly due to enhanced production or respiration, we examined the seasonal cycle of NPP and respiration separately. The INM model does not provide NPP output, so it is excluded in this part of analyses. For respiration, instead of directly adding all flux components such as R_h and fLuc for each model (which would be unnecessary and difficult since not all fluxes are provided), we defined R_h^* (dominated by R_h) such that

$$R_h^* = \text{NPP} - \text{NBP}. \tag{2}$$

Additionally, we analyzed the spatial patterns of NBP changes between future (2081–2090) and historical (1961–1970) period. We examined the peak seasons of carbon uptake and release by the biosphere, namely May–July and October–December averages, respectively. The difference between the two periods gives us an approximate representation of NBP amplitude change. We chose three-month averages for multi-model ensemble, because not all models simulate peak uptake in June and peak release in October. Monthly output of NBP, NPP and R_h^* (derived from NBP and NPP) from all models were first resampled to $2° \times 2°$ grids. Then the spatial and zonal means for both May–July and October–December were computed.

3 Results

3.1 Changes of CO_2 and NBP seasonal amplitude

The CMIP5 models project that the increase of CO_2 seasonal amplitude continues in the future. Figure 1a shows detrended and globally averaged monthly column atmospheric CO_2 from 1961 to 2099, averaged over nine models (no IPSL). The models project an increase of CO_2 seasonal amplitude (defined as max minus min in each year) by 74 % over 120 years, from 1.6 ppm during 1961–1970 to 2.7 ppm in 2081–2090. The increase is faster in the future than in historical period. Another feature is that the trend of minimums (-0.63 ppm century^{-1}) has a larger magnitude than the trend of maximums (0.41 ppm century^{-1}), suggesting that enhanced vegetation growth contributes more to the amplitude increase than higher respiration. Figure 1b and c present detrended global mean CO_2 growth rate (1 ppm = 2.12 Pg C month^{-1} for unit conversion) and $-$NBP, two quantities showing very similar characteristics as expected. All models simulate an increase in amplitude, although considerable model spread is found (Table 2). Excluding models beyond one standard deviation range yields similar results.

We further calculated the change of relative amplitude (relative to 1961–1970) for each model. Here amplitude is computed by the CCGCRV package. As illustrated in Fig. 2, all nine models show an increase in both global mean CO_2 and NBP seasonal amplitude. CO_2 seasonal amplitude has increased by 62 ± 19 % in 2081–2090, compared to 1961–1970; whereas NBP seasonal amplitude has increased by 68 ± 25 % over the same period (see Table 3 for details of individual models). The trend of increase is much higher in the future (CO_2/NBP: 0.70 %/0.73 % per year during 2006–2099) than in the historical period (0.25 and 0.28 % per year during 1961–2005 for CO_2 and NBP), albeit the model spread also becomes larger in the future.

To illustrate how well the models simulate the seasonal variations of CO_2, we compared the multi-model ensemble global CO_2 at the lowest model level – not equivalent to the height of surface CO_2 measurement, but relatively close – with ESRL's global

mean CO_2 over 1981–2005 (Fig. 1d). The surface CO_2 amplitude increase estimated by the models is lower than ESRL's global CO_2 estimate, however the changes of amplitude are similar (Table 4). This surface station-based global CO_2 estimate also indicates that the amplitude increase is dominated by the trend of minimums.

3.2 Phase change

Atmospheric CO_2 rises from fall (Northern Hemisphere) to early spring, when carbon uptake is smaller than release. The peak values are simulated to occur in April based on the multi-model ensemble. Then carbon uptake surpasses release, and global concentration decreases over spring and summer – the growing season of Northern Hemisphere biosphere – until reaching the minimum in September/August. This "clocklike" breathing behavior of biosphere will probably change: models simulate a shift of minimum CO_2 concentration occurrence from mixed September/August in the historical period to August in the future (Fig. 3a).

The minimums and maximums of the CO_2 growth rate and $-NBP$ (Fig. 3b and c) indicate the model-simulated months of maximum carbon imbalance associated with peak vegetation growth and decay. As shown in Fig. 3b, both the maximums and minimums of the CO_2 growth rate are more likely to be found at an earlier time of year, as if the biosphere clock is turning back: minimums occurred mostly in July, but shift to June in the second half of the 21st century; maximums were in November/January, but shift to more October in the last quarter of the 21st century. Similarly, peak carbon uptake by terrestrial biosphere (minimum $-NBP$, or maximum NBP) occurs in June, and peak carbon release shifts from March/January to October, November and January towards the end of the time series.

3.3 Production vs. respiration

Our next question is whether the amplitude change of NBP is largely driven by NPP or respiration. We computed the mean seasonal cycle of $-NBP$, $-NPP$ (reverse signs

so that negative values always indicate carbon uptake) and R_h^* in two periods: 1961–1970 (black) and 2081–2090 (red), for the nine models (for this and following analyses, we excluded INM which does not provide NPP, and included the IPSL model). The shaded areas represent model spread (one standard deviation). The seasonal ampli-tude of NBP, computed as max minus min (June–October), has increased from 2.7 to 4.7 $PgC\,month^{-1}$ (Fig. 4a). The 2 $PgC\,month^{-1}$ amplitude change is the sum of enhanced net carbon uptake in June and higher net release in October, and the up-take increase (1.4 $PgC\,month^{-1}$) is nearly three times as large as the release increase (0.5 $PgC\,month^{-1}$). The biggest increases of carbon uptake mostly take place during a short period from May to July, while carbon release shows a more even change from August to January.

We then investigate the June and October changes of –NPP and R_h^*, respec-tively. By definition, their sum should equal to the amplitude change of –NBP. NPP has increased in all months (Fig. 4b), with much larger changes during the North-ern Hemisphere growing season. The amplitude of NPP has increased from 4.8 to 7.1 $PgC\,month^{-1}$, and the amplitude of R_h^* from 2.7 to 4.3 $PgC\,month^{-1}$. In June, NPP increase (4.5 $PgC\,month^{-1}$) is larger than that of R_h^* (3.1 $PgC\,month^{-1}$), resulting in en-hanced net uptake. In October, NPP increase (1.9 $PgC\,month^{-1}$) is smaller than that of R_h^* (2.4 $PgC\,month^{-1}$), leading to enhanced net release. These results are consistent with trends of maximums and minimums in Fig. 1.The models also indicate a shift in peak NPP from July to June, consistent with the shift of CO_2 minimums.

3.4 Spatial and latitudinal contributions

To further investigate the regional contribution to NBP change, we plotted the 10-model mean –NBP changes (Fig. 5) over peak Northern Hemisphere growing season (May–July) and dormant season (October–December). Because the models disagree on the time of maximum and minimum NBP, our choice of doing seasonal averages would be more representative of the models than averaging over one month. We saw stronger

net carbon uptake in May–July almost everywhere north of 45° N, and also over the Tibetan Plateau and some places near equator. Net carbon uptake weakens over Western US and Central America, South and Southeast Asia and Central South America. The change of net carbon release in October–December generally shows an opposite spatial pattern, but the relative magnitude of change over 45–90° N is much smaller.

In addition, we calculated the zonal averages of the changes in May–July (black line) and October–December (red line). The green shaded areas contribute positively to the amplitude increase, whereas the yellow shades contribute negatively. It is apparent that the seasonal amplitude increase of NBP is dominated by regions north of 45° N with a weak contribution by the Southern Hemisphere tropics (−25–0° S). The Northern subtropical region and Southern Hemisphere (10–30° N, 55–35° S) partly offset the amplitude increase. It is also clear from this figure that the amplitude increase is dominated changes in peak growing season.

3.5 Relationship with mean carbon sink

Since CO_2 fertilization effect is a major mechanism causing the amplitude increase, we expect models with a larger change in mean carbon sink would simulate a larger change in seasonal amplitude. By plotting the −NBP change against NBP seasonal amplitude change for all 10 models (Fig. 6), we found there is indeed a negative correlation ($R = -0.73$, $p < 0.05$), indicating models with enhanced net carbon sink are likely to simulate a larger change in NBP seasonal amplitude. Again all models show an increase in NBP seasonal amplitude, even though they disagree on the direction of future NBP change. While our study hint at the relationship between mean carbon sink and seasonal amplitude, it is beyond our scope to discuss further on why models show such different mean sink estimate. Interested readers may refer to the insightful discussion on this issue in Friedlingstein et al. (2013).

4   Discussions and conclusions

Under the RCP8.5 emission scenario, all models we examined project an increase in seasonal amplitude of both CO_2 and NBP. In addition, the models indicate an earlier onset and peak of Northern Hemisphere biosphere growth and decay under future climate and CO_2 conditions. The year-to-year variability in simulated amplitude is large in many models, possibly reflecting the models' sensitivity to climate variations. Our analyses also suggest the amplitude increase is dominated by changes in net primary productivity, and in regions north of 45° N. While we focused on the change of amplitude instead of mean carbon sink (a more frequently discussed topic), our results suggest models simulating a stronger mean carbon sink are likely to project a larger change in NBP seasonal amplitude. Considerable model spread is found, likely due to different model setup and complexity, different climate conditions simulated by the models, sensitivity to CO_2 and climate and their combined effects, and strength of feedbacks. Our findings indicate factors including enhanced CO_2 fertilization and lengthening of growing season in high-latitude regions outcompetes the loss of biosphere productivity due to possible severe drought and forest degradation in the future, according to the CMIP5 models we studied.

Despite of high consistency on amplitude increase, the results of the models are highly uncertain. On one hand, the simulated future amplitude increase may be on the high side, because the RCP8.5 scenario is used to drive the ESMs. Also, the emission-driven runs simulate higher CO_2 than observed over the historical period, and such biases are likely to increase through time as the atmospheric CO_2 growth rate accelerates (Hoffman et al., 2014). On the other hand, the models may underestimate the historical amplitude increase, because apart from CO_2 fertilization and lengthening of high latitude growing season, other factors at play for the past may not be represented in the CMIP5 models (Graven et al., 2013; Zeng et al., 2014). Therefore, it is unlikely that models have accounted for all important factors in the future simulations.

A logical next step is to understand the underlying mechanisms for the amplitude change – the contribution of CO_2 fertilization, high latitude warming and other factors. CMIP5 has recommended additional experiments for this purpose: Fixed Feedback 2 (esmFdbk2) and Fixed Climate 2 (esmFixClim2). The former keeps CO_2 concentra-
tion fixed but allow physical climate change responding to increasing historical and future (RCP4.5) concentrations; the latter keeps climate fixed under preindustrial CO_2 condition but allow the carbon cycle to respond to historical and future (RCP4.5) CO_2 increase. We found it difficult to separate the contribution of CO_2 fertilization and high latitude warming with this setup: one major difference is the use of RCP4.5 concentra-
tions instead of RCP8.5 emissions. Also, much fewer modeling groups have submitted results for these two experiments (only 4 out of the 10 models we examined). For such reasons, we are unlikely to draw meaningful conclusions by analyzing the output of four models for the two additional experiments.

Fortunately, other model intercomparison projects like TRENDY (http://dgvm.ceh.ac.
uk) and MsTMIP (http://nacp.ornl.gov/MsTMIP.shtml) have designed sets of sensitivity experiments to isolate the influencing factors. Models participating in these two projects are not fully coupled to simulate both climate and carbon cycle changes; instead they are forced by observed climate, CO_2 and land use conditions, simulating only for the historical period and aiming at understanding the past. We plan to use model output from these two projects to investigate the contribution of CO_2 fertilization, high latitude warming and other factors in future studies. It is our hope that improved understandings of the past would shed light on how the Earth's ecosystem would adjust its "breathing" under future environmental changes.

Title Page

Abstract | Introduction

Conclusions | References

Tables | Figures

◄ | ►◄

◄ | ►

Back | Close

Full Screen / Esc

Printer-friendly Version

Interactive Discussion

References

Andres, R. J., Gregg, J. S., Losey, L., Marland, G., and Boden, T. A.: Monthly, global emissions of carbon dioxide from fossil fuel consumption, Tellus B, 63, 309–327, doi:10.1111/j.1600-0889.2011.00530.x, 2011.

Arora, V. K., Scinocca, J. F., Boer, G. J., Christian, J. R., Denman, K. L., Flato, G. M., Kharin, V. V., Lee, W. G., and Merryfield, W. J.: Carbon emission limits required to satisfy future representative concentration pathways of greenhouse gases, Geophys. Res. Lett., 38, L05805, doi:10.1029/2010GL046270, 2011.

Bacastow, R. B., Keeling, C. D., and Whorf, T. P.: Seasonal amplitude increase in atmospheric CO_2 Concentration at Mauna Loa, Hawaii, 1959–1982, J. Geophys. Res., 90, 10529–10540, 1985.

Buermann, W., Lintner, B. R., Koven, C. D., Angert, A., Pinzon, J. E., Tucker, C. J., and Fung, I. Y.: The changing carbon cycle at Mauna Loa Observatory, P. Natl. Acad. Sci. USA, 104, 4249–4254, 2007.

Cleveland, W., Freeny, A. E., and Graedel, T. E.: The seasonal component of atmospheric CO_2: information from new approaches to the decomposition of seasonal time series, J. Geophys. Res., 88, 10934–10946, 1983.

Conway, J. T., Tans, P. P., Waterman, L. S., Thoning, K. W., Kitzis, D. R., Masarie, K. A., and Zhang, N.: Evidence for interannual variability of the carbon cycle from the National Oceanic and Atmospheric Administration/Climate Monitoring and Diagnostics Laboratory Global Air Sampling Network, J. Geophys. Res., 99, 22831–22855, 1994.

Dufresne, J.-L., Foujols, M.-A., Denvil, S., Caubel, A., Marti, O., Aumont, O., Balkanski, Y., Bekki, S., Bellenger, H., Benshila, R., Bony, S., Bopp, L., Braconnot, P., Brockmann, P., Cadule, P., Cheruy, F., Codron, F., Cozic, A., Cugnet, D., Noblet, N., Duvel, J.-P., Ethé, C., Fairhead, L., Fichefet, T., Flavoni, S., Friedlingstein, P., Grandpeix, J.-Y., Guez, L., Guilyardi, E., Hauglustaine, D., Hourdin, F., Idelkadi, a., Ghattas, J., Joussaume, S., Kageyama, M., Krinner, G., Labetoulle, S., Lahellec, A., Lefebvre, M.-P., Lefevre, F., Levy, C., Li, Z. X., Lloyd, J., Lott, F., Madec, G., Mancip, M., Marchand, M., Masson, S., Meurdesoif, Y., Mignot, J.,

Musat, I., Parouty, S., Polcher, J., Rio, C., Schulz, M., Swingedouw, D., Szopa, S., Talandier, C., Terray, P., Viovy, N., and Vuichard, N.: Climate change projections using the IPSL-CM5 Earth System Model: from CMIP3 to CMIP5, Clim. Dynam., 40, 2123–2165, doi:10.1007/s00382-012-1636-1, 2013.

5 Dunne, J. P., John, J. G., Shevliakova, E., Stouffer, R. J., Krasting, J. P., Malyshev, S. L., Milly, P. C. D., Sentman, L. T., Adcroft, A. J., Cooke, W., Dunne, K. A., Griffies, S. M., Hallberg, R. W., Harrison, M. J., Levy, H., Wittenberg, A. T., Phillips, P. J. and Zadeh, N.: GFDL's ESM2 Global Coupled Climate–Carbon Earth System Models. Part II: Carbon system formulation and baseline simulation characteristics, J. Climate, 26, 2247–2267, doi:10.1175/JCLI-
10 D-12-00150.1, 2013.

Friedlingstein, P., Meinshausen, M., Arora, V. K., Jones, C. D., Anav, A., Liddicoat, S. K., and Knutti, R.: Uncertainties in CMIP5 climate projections due to carbon cycle feedbacks, J. Climate, 27, 511–526, doi:10.1175/JCLI-D-12-00579.1, 2013.

Graven, H. D., Keeling, R. F., Piper, S. C., Patra, P. K., Stephens, B. B., Wofsy, S. C., Welp, L. R.,
15 Sweeney, C., Tans, P. P., Kelley, J. J., Daube, B. C., Kort, E. A, Santoni, G. W., and Bent, J. D.: Enhanced seasonal exchange of CO_2 by northern ecosystems since 1960, Science, 341, 1085–1089, doi:10.1126/science.1239207, 2013.

Hoffman, F. M., Randerson, J. T., Arora, V. K., Bao, Q., Cadule, P., Ji, D., Jones, C. D., Kawamiya, M., Khatiwala, S., Lindsay, K., Obata, A., Shevliakova, E., Six, K. D., Tjiputra, J. F., Volodin, E. M., and Wu, T.: Causes and implications of persistent atmospheric
20 carbon dioxide biases in Earth System Models, J. Geophys. Res.-Biogeosci., 119, 141–162, doi:10.1002/2013JG002381, 2014.

Ilyina, T., Six, K. D., Segschneider, J., Maier-Reimer, E., Li, H, and Núñez-Riboni, I: Global ocean biogeochemistry model HAMOCC?: model architecture and performance as compo-
25 nent of the MPI-Earth system model in different CMIP5 experimental realizations, J. Adv. Model. Earth Syst., 5, 287–315, doi:10.1029/2012MS000178, 2013.

International Panel on Climate Change: Climate Change 2013: the Physical Science Basis. Working Group I Contribution to the Fifth Assessment Report of the International Panel on Climate Change International Panel on Climate Change, Cambridge University Press, Cam-
30 bridge, United Kingdom and New York, NY, USA, 2013.

Ji, D., Wang, L., Feng, J., Wu, Q., Cheng, H., Zhang, Q., Yang, J., Dong, W., Dai, Y., Gong, D., Zhang, R.-H., Wang, X., Liu, J., Moore, J. C., Chen, D., and Zhou, M.: Description and

basic evaluation of BNU-ESM version 1, Geosci. Model Dev. Discuss., 7, 1601–1647, doi:10.5194/gmdd-7-1601-2014, 2014.

Keeling, C. D., Whorf, T. P., Wahlen, M., and van der Plichtt, J.: Interannual extremes in the rate of rise of atmospheric carbon dioxide since 1980, Nature, 375, 666–670, doi:10.1038/375666a0, 1995.

Keeling, C. D., Chin, J. F. S., and Whorf, T. P.: Increased activity of northern vegetation inferred from atmospheric CO_2 measurements, Nature, 382, 146–149, doi:10.1038/382146a0, 1996.

Kohlmaier, G. H., Siré, E. O., Janecek, A., Keeling, C. D., Piper, S. C., and Revelle, R.: Modelling the seasonal contribution of a CO_2 fertilization effect of the terrestrial vegetation to the amplitude increase in atmospheric CO_2 at Mauna Loa Observatory, Tellus B, 41, 487–510, doi:10.1111/j.1600-0889.1989.tb00137.x, 1989.

Long, M. C., Lindsay, K., Peacock, S., Moore, J. K., and Doney, S. C.: Twentieth-century oceanic carbon uptake and storage in CESM1(BGC), J. Climate, 26, 6775–6800, doi:10.1175/JCLI-D-12-00184.1, 2013.

McGuire, A. D., Sitch, S., Clein, J. S., Dargaville, R., Esser, G., Foley, J., Heimann, M., Joos, F., Kaplan, J., Kicklighter, D. W., Meier, R. A, Melillo, J. M., Moore, B., Prentice, I. C., Ramankutty, N., Reichenau, T., Schloss, A., Tian, H., Williams, L. J., and Wittenberg, U.: Carbon balance of the terrestrial biosphere in the twentieth century: analyses of CO_2, climate and land use effects with four process-based ecosystem models, Global Biogeochem. Cy., 15, 183–206, 2001.

Moss, R. H., Edmonds, J. A., Hibbard, K. A., Manning, M. R., Rose, S. K., van Vuuren, D. P., Carter, T. R., Emori, S., Kainuma, M., Kram, T., Meehl, G. A., Mitchell, J. F. B., Nakicenovic, N., Riahi, K., Smith, S. J., Stouffer, R. J., Thomson, A. M., Weyant, J. P., and Wilbanks, T. J.: The next generation of scenarios for climate change research and assessment, Nature, 463, 747–756, doi:10.1038/nature08823, 2010.

Pearman, G. I. and Hyson, P.: The annual variation of atmospheric CO_2 concentration observed in the Northern Hemisphere, J. Geophys. Res., 86, 9839–9843, 1981.

Piao, S., Sitch, S., Ciais, P., Friedlingstein, P., Peylin, P., Wang, X., Ahlström, A., Anav, A., Canadell, J. G., Cong, N., Huntingford, C., Jung, M., Levis, S., Levy, P. E., Li, J., Lin, X., Lomas, M. R., Lu, M., Luo, Y., Ma, Y., Myneni, R. B., Poulter, B., Sun, Z., Wang, T., Viovy, N., Zaehle, S., and Zeng, N.: Evaluation of terrestrial carbon cycle models for their response to climate variability and to CO_2 trends, Glob. Change. Biol., 19, 2117–2132, doi:10.1111/gcb.12187, 2013.

Discussion Paper | Discussion Paper | Discussion Paper | Discussion Paper | Discussion Paper

Title Page

Abstract | Introduction

Conclusions | References

Tables | Figures

|◄ | ►|

◄ | ►

Back | Close

Full Screen / Esc

Printer-friendly Version

Interactive Discussion

Randerson, J. T., Thompson, M. V., Conway, T. J., Fung, I. Y., and Field, C. B.: The contribution of terrestrial sources and sinks to trends in the seasonal cycle of atmospheric carbon dioxide, Global Biogeochem. Cy., 11, 535–560, 1997.

Randerson, J. T., Field, C. B., Fung, I. Y., and Tans, P. P.: Increases in early season ecosystem uptake explain recent changes in the seasonal cycle of atmospheric CO_2 at high northern latitudes, Geophys. Res. Lett., 26, 2765–2768, doi:10.1029/1999GL900500, 1999.

Taylor, K. E., Stouffer, R. J., and Meehl, G. A.: An overview of CMIP5 and the experiment design, B. Am. Meteorol. Soc., 93, 485–498, doi:10.1175/BAMS-D-11-00094.1, 2012.

Thoning, K. W., Tans, P. P., and Komhyr, W. D.: Atmospheric carbon dioxide at Mauna Loa Observatory 2. Analysis of the NOAA GMCC data, 1974–1985, J. Geophys. Res., 94, 8549–8565, 1989.

Tjiputra, J. F., Roelandt, C., Bentsen, M., Lawrence, D. M., Lorentzen, T., Schwinger, J., Seland, Ø., and Heinze, C.: Evaluation of the carbon cycle components in the Norwegian Earth System Model (NorESM), Geosci. Model Dev., 6, 301–325, doi:10.5194/gmd-6-301-2013, 2013.

Volodin, E. M., Dianskii, N. A., and Gusev, A. V.: Simulating present-day climate with the IN-MCM4.0 coupled model of the atmospheric and oceanic general circulations, Izv. Atmos. Ocean. Phy., 46, 414–431, doi:10.1134/S000143381004002X, 2010.

Watanabe, S., Hajima, T., Sudo, K., Nagashima, T., Takemura, T., Okajima, H., Nozawa, T., Kawase, H., Abe, M., Yokohata, T., Ise, T., Sato, H., Kato, E., Takata, K., Emori, S., and Kawamiya, M.: MIROC-ESM 2010: model description and basic results of CMIP5-20c3m experiments, Geosci. Model Dev., 4, 845–872, doi:10.5194/gmd-4-845-2011, 2011.

Williams, D. N., Taylor, K. E., Cinquini, L., Evans, B., Kawamiya, M., Lawrence, B. N., and Middleton, D. E.: The Earth System Grid Federation: software framework supporting CMIP5 data analysis and dissemination, CLIVAR Exchanges, 16, 40–42, 2011.

Yukimoto, S., Yoshimura, H., Hosaka, M., Sakami, T., Tsujino, H., Hirabara, M., Tanaka, T. Y., Deushi, M., Obata, A., Nakano, H., Adachi, Y., Shindo, E., Yabu, S., Ose, T., and Kitoh, A.: Meteorological Research Institute-Earth System Model Version 1 (MRI-ESM1)-model description, Tech. Rep. 64, Meteorological Research Institute, 2011.

Zeng, N., Zhao, F., Collatz, G. J., Kalnay, E., Salawitch, R. J., West, T. O., and Guanter, L.: Increasing atmospheric CO_2 seasonal amplitude: contribution from the agricultural Green Revolution since 1961, Nature, under review, 2014.

Zimov, S. A., Davidov, S. P., Zimova, G. M., Davidova, A. I., Chapin, F. S., Chapin, M. C., and Reynolds, J. F.: Contribution of disturbance to increasing seasonal amplitude of atmospheric CO_2, Science, 284, 1973–1976, doi:10.1126/science.284.5422.1973, 1999.

Title Page

Abstract | Introduction

Conclusions | References

Tables | Figures

|◄ | ►|

◄ | ►

Back | Close

Full Screen / Esc

Printer-friendly Version

Interactive Discussion

Table 1. List of models used and their characteristics.

Models	Modeling Center	Land Component	Resolution (Lon × Lat)	Reference
BNU-ESM	Beijing Normal University, China	CoLM3	2.8125° × 2.8125°	Ji et al. (2014)
CanESM2	Canadian Centre for Climate Modeling and Analysis, Canada	CTEM	2.8125° × 2.8125°	Arora et al. (2011)
CESM1-BGC	Community Earth System Model Contributors, NSF-DOE-NCAR, USA	CLM4	1.25° × 0.9°	Long et al. (2013)
GFDL-ESM2m	NOAA Geophysical Fluid Dynamics Laboratory, USA	LM3	2.5° × 2°	Dunne et al. (2013)
INM-CM4	Institute for Numerical Mathematics, Russia		2° × 1.5°	Volodin et al. (2010)
IPSL-CM5A-LR	Institut Pierre-Simon Laplace, France	ORCHIDEE	3.75° × 1.875°	Dufresne et al. (2013)
MIROC-ESM	Japan Agency for Marine-Earth Science and Technology, Atmosphere and Ocean Research Institute (University of Tokyo), and National Institute for Environmental Studies, Japan	MATSIRO + SEIB-DGVM	2.8125° × 2.8125°	Watanabe et al. (2011)
MPI-ESM-LR	Max Planck Institute for Meteorology, Germany	JSBACH	2.8125° × 2.8125°	Ilyina et al. (2013)
MRI-ESM1	Meteorological Research Institute, Japan	HAL	1.125° × 1.125°	Yukimoto et al. (2011)
NorESM1-ME	Norwegian Climate Centre, Norway	CLM4	2.5° × 1.875°	Tjiputra et al. (2013)

Table 2. Amplitude (max minus min) of global mean column atmospheric CO_2, CO_2 growth rate (CO_2g) and global total NBP, averaged over 1961–1970 and 2081–2090 for the nine models, and their multi-model ensemble (MME) and standard deviation (SD).

Models	CO_2 (ppm)		CO_2g (Pg C month^{-1})		$-NBP$ (Pg C month^{-1})	
	1961–1970	2081–2090	1961–1970	2081–2090	1961–1970	2081–2090
BNU-ESM	1.54	2.96	2.2	4.91	1.88	4.42
CanESM2	0.9	1.53	1.12	2.05	1.2	1.83
CESM1-BGC	1.2	1.76	1.51	2.59	1.6	2.38
GFDL-ESM2m	2.37	3.81	3.42	5.93	3.52	6.24
INM-CM4	0.27	0.41	0.38	0.57	0.3	0.49
MIROC-ESM	2.55	3.92	3.93	5.98	3.77	5.37
MPI-ESM-LR	3.45	5.47	4.35	6.37	4.61	7.51
MRI-ESM1	1.97	4.04	2.37	5.21	2.63	5.7
NorESM1-ME	1.23	1.8	1.6	2.63	1.74	2.73
MME[*]	1.72	2.86	2.32	4.03	2.36	4.07
SD	0.97	1.59	1.34	2.09	1.38	2.33

[*] The multi-model ensemble (MME) here is a simple average over the nine models in the table. The values are slightly larger than given in text because of averaging method (in the main text, multi-model averaging of detrended variables are done first, then their amplitude are computed and mean amplitude changes are derived).

Table 3. Column atmospheric CO_2 and NBP amplitude (computed by CCGCRV, slightly different from max minus min) Increases of nine models by 2081–2090 relative to their 1961–1970 values and their multi-model ensemble (MME).

Models	CO_2	NBP
BNU-ESM	93 %	113 %
CanESM2	65 %	47 %
CESM1-BGC	46 %	47 %
GFDL-ESM2m	57 %	79 %
INM-CM4	51 %	67 %
MIROC-ESM	52 %	39 %
MPI-ESM-LR	54 %	58 %
MRI-ESM1	99 %	106 %
NorESM1-ME	45 %	58 %
MME	62 %	68 %

Table 4. Amplitude change (ppm) and trends of maximums/minimums of surface CO_2 from eight models, their multi-model ensemble (MME), and ESRL's Global mean CO_2 (CO_2GL).

Models	1981–1985 (ppm)	2001–2005 (ppm)	Percent Change	Trend of Minimums (ppm 10 yr^{-1})	Trend of Maximums (ppm 10 yr^{-1})
BNU-ESM	2.71	3.1	14.39 %	−0.099	0.096
CanESM2	3.04	3.24	6.58 %	−0.064	0.02
CESM1-BGC	2.05	2.18	6.34 %	−0.032	0.044
GFDL-ESM2m	3.71	3.76	1.35 %	−0.033	0.095
MIROC-ESM	3.39	3.61	6.49 %	−0.078	0.045
MPI-ESM-LR	6.19	7.02	13.41 %	−0.25	0.171
MRI-ESM1	3.69	3.85	4.34 %	−0.095	0.031
NorESM1-ME	2.37	2.47	4.22 %	−0.024	0.016
MME	3.1	3.37	8.71 %	−0.084	0.065
CO_2 GL	4.11	4.4	7.06 %	−0.102	0.024
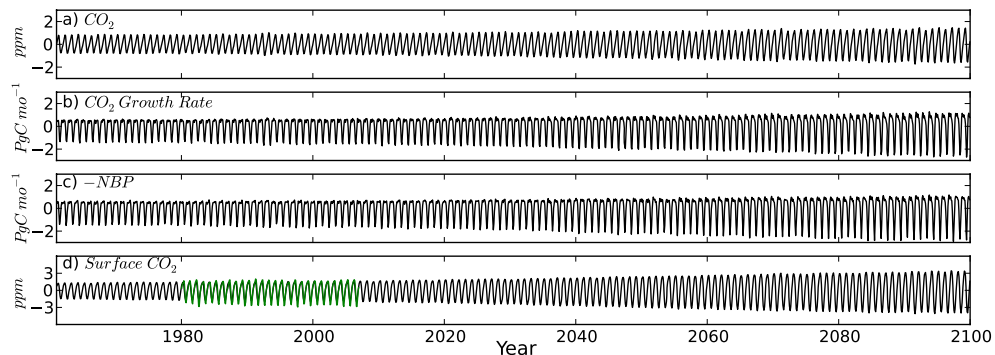
Figure 1. Nine-model (excluding IPSL) averaged monthly detrended **(a)**. Global mean CO_2 (ppm, column average); **(b)**. Global mean CO_2 growth rate (Pg C month^{-1}); and **(c)**. Global total −NBP (Pg C month^{-1}) from 1961 to 2099. **(d)** presents Eight-model (excluding IPSL and INM) averaged monthly detrended global mean CO_2 (ppm) at lowest model level and ESRL's global mean detrended surface CO_2 observation (shown in green).
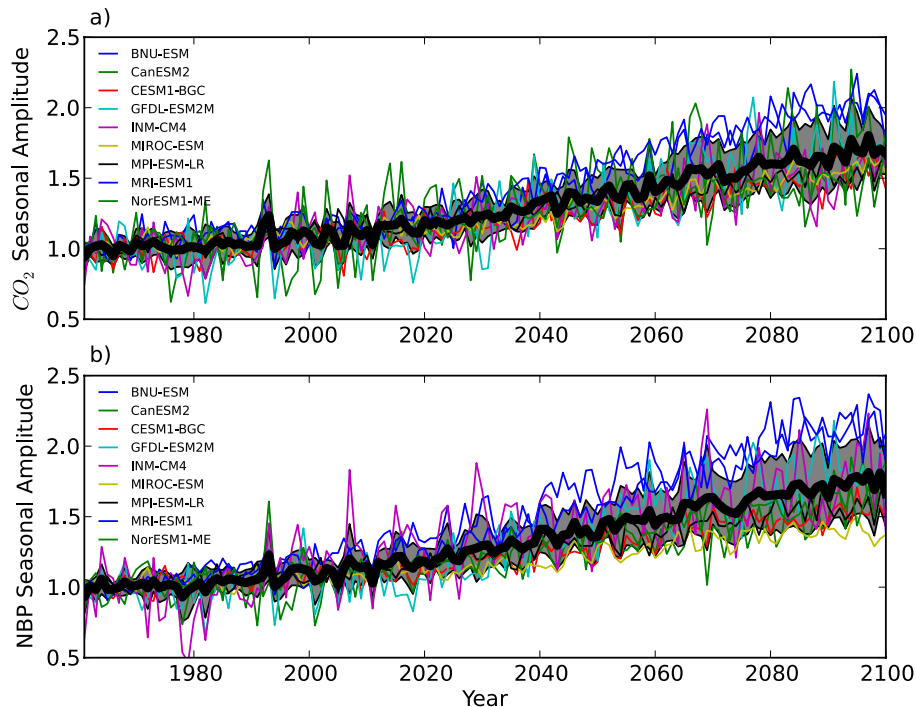
Figure 2. Time series of the relative seasonal amplitude (relative to 1961–1970 mean) of **(a)**. Global mean atmospheric CO_2 and **(b)**. Global total NBP from 1961 to 2099. Thick black line represents multi-model ensemble, and one standard deviation model spread is indicated by grey shade.

Full Screen / Esc

Printer-friendly Version

Interactive Discussion
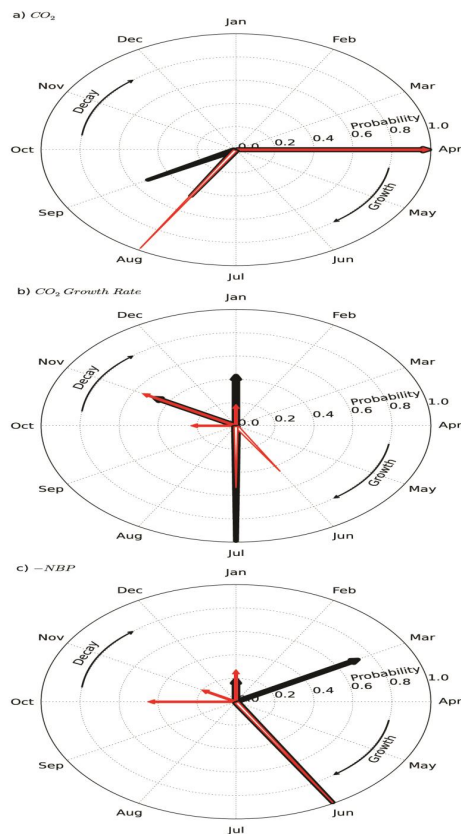
Figure 3. Phase change of seasonal cycles associated with growth and decay of biosphere: **(a).** CO_2; **(b).** CO_2 growth rate; and **(c).** −NBP. The arrows and wedges represent maximums and minimums, respectively. Their length denotes their probabilities of occurring in their pointed months (not shown if probability < 0.1). Historical (1961–2005) period is represented in black, and future (2006–2099) in red. Future maximums and minimums seem to occur at an earlier time of the year, as if the annual clock of biosphere is turning back.
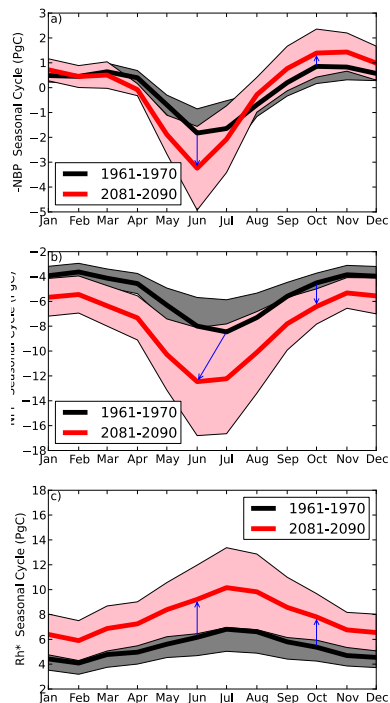
Figure 4. Nine-model mean (excluding INM) seasonal cycle of global total **(a)**. −NBP; **(b)** −NPP; and **(c)**. R_h^* (computed as NPP-NBP), averaged over 1961–1970 (red) and 2081–2090 (black). Shades indicate one standard deviation range among the models. Blue arrows mark the changes in June and October (maximum and minimum values of NBP). We show −NBP and −NPP so that the negative values represent carbon uptake by the biosphere, and positive values indicate carbon release from the biosphere.
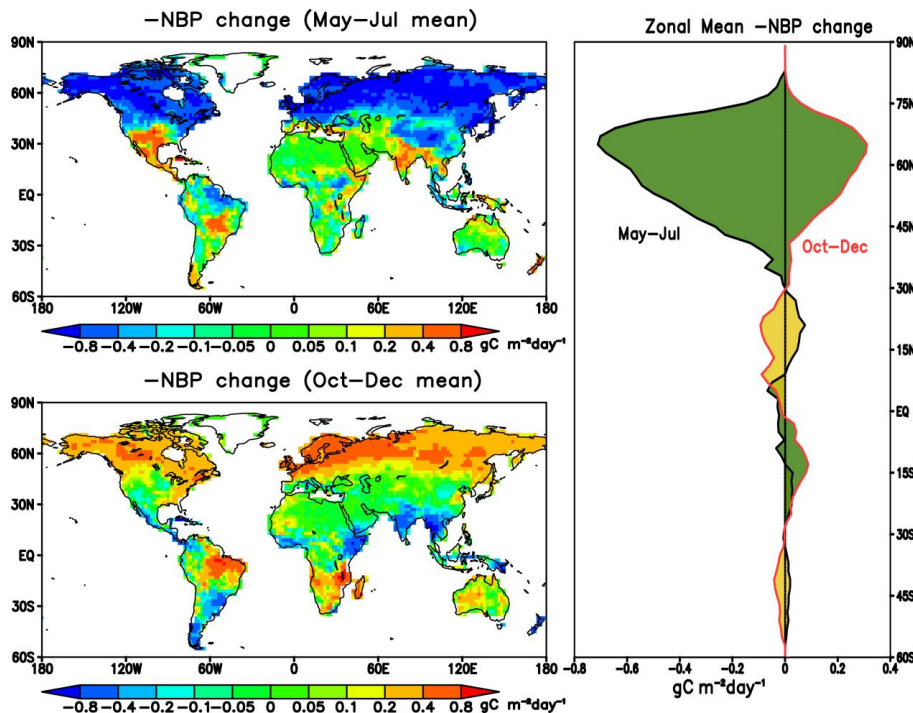
Figure 5. Spatial patterns and Latitudinal distributions of 10-model mean −NBP (g C m^{-2} day^{-1}) changes between 2081–2090 and 1961–1970, during mean peak growing season (May–July) and dormant season (October–December). Further reduction of −NBP in peak growing season (where the black curve falls below zero) and increase of −NBP in dormant season (where the red curve goes above zero) both contribute to amplitude increase, shaded in green in the zonal mean plot. The reversed case, shaded in yellow, indicates changes in regions that reduce seasonal amplitude. It is clear that the amplitude increase is dominated by the boreal regions, and by changes in peak growing season.
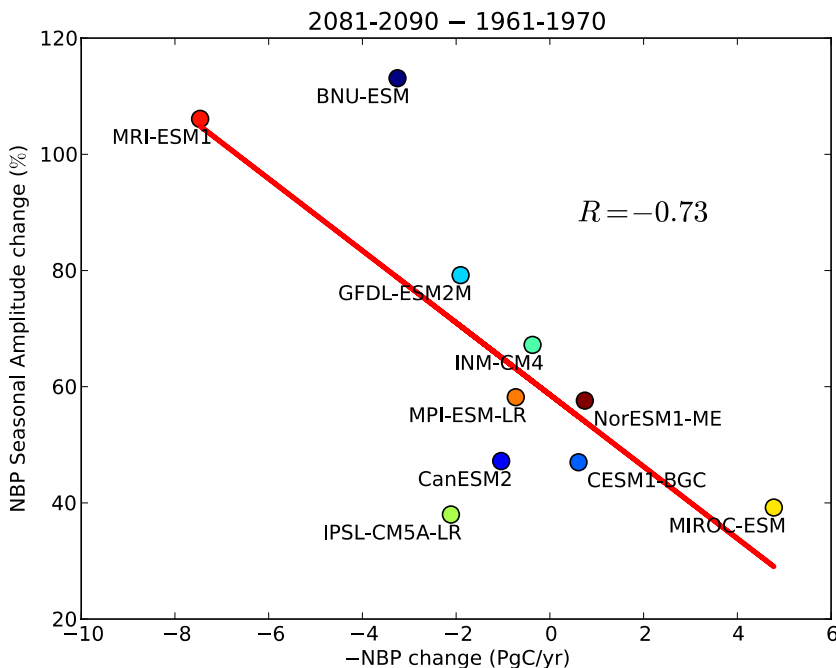
Figure 6. Relationship between −NBP change and change of NBP seasonal amplitude, calculated as the differences between 2081–2090 and 1961–1970 for the 10 CMIP5 ESMs. A negative correlation ($R = -0.73$, $p < 0.05$) is found, suggesting models with enhanced net carbon sink are likely to simulate a larger change in NBP seasonal amplitude.